3086 *Inorg. Chem.* **2010**, *49*, 3086–3088
DOI: 10.1021/ic902577r

Inorganic Chemistry
Communication

π-Back-Donation Effect of the Cyanide Ligands on the Electron Correlation and Charge Transfer in Prussian Blue $RbMn[Fe(CN)_6]$

Chuan Tian, Erjun Kan, Changhoon Lee, and Myung-Hwan Whangbo*

Department of Chemistry, North Carolina State University, Raleigh, North Carolina 27695-8204

Received December 26, 2009

The temperature-induced charge transfer between the Mn and Fe sites in $RbMn[Fe(CN)_6]$ was analyzed by density functional theory calculations. Our analysis indicates that the extent of electron correlation (equivalently, the pairing energy or the on-site repulsion) is much greater for the Mn^{n+} ion than for the Fe^{n+} ion ($n = 2, 3$). This surprising and counterintuitive finding is a consequence of the π-back-donation effect of the CN ligands.

Intense research efforts have been devoted to the structural and physical properties that can be controlled by changing the valency of their transition-metal ions.[1] In Prussian blues consisting of two different transition-metal ions,[2,3] charge transfer between them, and hence a change in their valency, can be induced by temperature,[4] photoexcitation,[5] pressure,[6] and electric field.[7] Such materials with controllable charge transfer are potentially important in multifunctional device applications. Among Prussian blues, $RbMn[Fe(CN)_6]$ is unique because it is stoichiometric and hence suitable for precise structural analyses. This compound consists of $Fe(CN)_6$ and $Mn(NC)_6$ octahedra, which share their CN ligands to form the double-perovskite framework with Fe−CN−Mn linkages (Figure 1). The Rb^+ ions occupy every second Mn_4Fe_4 cube such that the Rb^+ ions form a three-dimensional network of edge-sharing Rb_4 tetrahedra (Figure 1b).

$RbMn[Fe(CN)_6]$ undergoes a structural transition from the high-temperature (HT) cubic phase to the low-temperature (LT) tetragonal phase at 231 K upon a lowering of the temperature, while the LT phase is converted to the HT phase at 304 K upon a raising of the temperature.[4,8] In the HT cubic phase, both the $Fe(CN)_6$ and $Mn(NC)_6$ octahedra are regular in shape [Mn−N = 2.012 (×6) Å and Fe−C = 2.170 (×6) Å].[4] In the LT tetragonal phase, each $Mn(NC)_6$ octahedron shows a strong axial elongation [Mn−N = 1.991 (×4) and 2.268 (×2) Å] and each $Fe(CN)_6$ octahedron a slight axial flattening [Fe−C = 1.886 (×4) and 1.831 (×2) Å].[4] Experimental studies reveal that the LT phase has high-spin (HS) Mn^{3+} (d^4, $S = 2$) and low-spin (LS) Fe^{2+} (d^6, $S = 0$) ions, while the HT phase has HS Mn^{2+} (d^5, $S = {}^5/_2$) and LS Fe^{3+} (d^5, $S = {}^1/_2$) ions.[4,8] Namely, the temperature-induced phase transition involves charge transfer between the Mn and Fe sites.

The HS Mn^{3+}/LS Fe^{2+} configuration of the LT phase has been confirmed by electronic structure calculations,[8,9] but there has been no such report concerning the HS Mn^{2+}/LS Fe^{3+} configuration of the HT phase. In a discussion of the charge-transfer phenomenon of $RbMn[Fe(CN)_6]$, it is essential that the electronic structures of both the HT and LT phases be equally well described under a given theoretical analysis. This need prompted us to carry out a systematic density functional theory (DFT) study of the HT and LT phases. In the present Communication, we report surprising results of our investigation, which reveal that the extent of electron correlation is much greater for the Mn^{n+} ion than for the Fe^{n+} ion ($n = 2, 3$) in $RbMn[Fe(CN)_6]$, and this counterintuitive finding is a consequence of the π-back-donation effect of the CN ligands.

Our spin-polarized DFT calculations, for the experimental structures of the LT and HT phases unless otherwise

*To whom correspondence should be addressed. E-mail: mike_whangbo@ncsu.edu.

(1) (a) Long, Y.; Hayashi, N.; Saito, T.; Azuma, M.; Muranaka, S.; Shimakawa, Y. *Nature* **2008**, *458*, 60. (b) Imada, M.; Fujimori, A.; Tokura, Y. *Rev. Mod. Phys.* **1998**, *70*, 1039.
(2) (a) Sato, O.; Iyoda, T.; Fujishima, A.; Hashimoto, K. *Science* **1996**, *272*, 704. (b) Sato, O.; Iyoda, T.; Fujishima, A.; Hashimoto, K. *Science* **1996**, *271*, 49. (c) Coronado, E.; Galan-Mascaros, J. R.; Gomez-Garcia, C. J.; Laukhin, V. *Nature* **2000**, *408*, 447.
(3) (a) Manriquez, J. M.; Yee, G. T.; Mclean, R. S.; Epstein, A. J.; Miller, J. S. *Science* **1991**, *252*, 1415. (b) Ferlay, S.; Mallah, T.; Ouahes, R.; Veillet, P.; Verdagure, M. *Nature* **1995**, *378*, 701.
(4) (a) Ohkoshi, S.; Tokoro, H.; Utsunomiya, M.; Mizuno, M.; Abe, M.; Hashimoto, K. *J. Phys. Chem. B* **2002**, *106*, 2423. (b) Moritomo, Y.; Kato, K.; Kuriki, A.; Takata, M.; Sakata, M.; Tokoro, H.; Ohkoshi, S.; Hashimoto, K. *J. Phys. Soc. Jpn.* **2002**, *71*, 2078.
(5) (a) Liu, X.; Moritomo, Y.; Ichida, M.; Nakamura, A.; Kojima, N. *Phys. Rev. B* **2000**, *61*, 20. (b) Margadonna, S.; Prassides, K.; Fitch, A. *Angew. Chem., Int. Ed.* **2004**, *43*, 6316.
(6) Moritomo, Y.; Hanawa, M.; Ohishi, Y.; Kato, K.; Takata, M.; Nishibori, E.; Sakata, M.; Ohkoshi, S.; Tokoro, H.; Hashimoto, K. *Phys. Rev. B* **2003**, *68*, 144106.
(7) Mahfoud, H.; Molnar, G.; Bonhommeau, S.; Cobo, S.; Salmon, L.; Demont, P.; Tokoro, H.; Ohkoshi, S.; Boukheddaden, K.; Bousseksou, A. *J. Am. Chem. Soc.* **2009**, *131*, 15049.
(8) Kato, K.; Moritomo, Y.; Takata, M.; Sakata, M.; Umekawa, M.; Hamada, N.; Ohkoshi, S.; Tokoro, H.; Hashimoto, K. *Phys. Rev. Lett.* **2003**, *91*, 255502.
(9) Umekawa, M.; Hamada., N.; Kodama, A.; Moritomo, Y. *J. Phys. Soc. Jpn.* **2004**, *73*, 430.

 Published on Web 03/03/2010

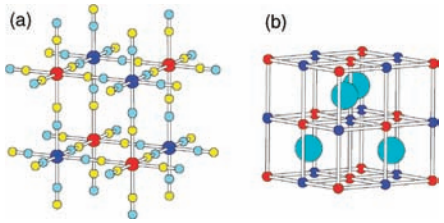

Figure 1. (a) Perspective view of the crystal structure of the HT cubic phase of $RbMn[Fe(CN)_6]$. The red and blue circles represent the Fe and Mn atoms, respectively, and the yellow and turquoise circles the C and N atoms, respectively. (b) Arrangement of the Rb atoms in the Mn_4Fe_4 cubes.

mentioned, employed the projector-augmented wave method implemented in the Vienna ab initio simulation package[10] with the generalized gradient approximation (GGA),[11] a plane-wave cutoff energy of 400 eV, a set of $3 \times 3 \times 3$ k points,[12] and a threshold of 10^{-6} eV for energy convergence. In general, band gaps are underestimated and the electron localization of 3d states is poorly described by DFT calculations. These deficiencies are commonly corrected by performing either DFT+U[13] or hybrid-functional[14] calculations. In the hybrid-functional method, the exchange energy is obtained by mixing the Hartree−Fock and DFT exchange energies in a certain ratio. In the DFT+U method, the on-site repulsion U is added on magnetc transition-metal ions. Our study adopted the DFT+U method of Dudarev et al.,[13] which makes use of the effective on-site repulsion $U_{eff} = U - J$, where the screened exchange parameter J is on the order of 0.9 eV. In our GGA+U calculations, the U_{eff} values on Mn and Fe are referred to as U_{Mn} and U_{Fe}, respectively.

Because $RbMn[Fe(CN)_6]$ has two different transition elements, Mn and Fe, it is not a trivial task to find the appropriate U_{Mn} and U_{Fe} values for the GGA+U calculations especially when both atoms possess unpaired spins, as is found for the HT phase. In their elemental state, Mn has less contracted 3d orbitals than does Fe so that U_{Fe} and U_{Mn} would be comparable in magnitude with $U_{Mn} < U_{Fe}$. Thus, we begin our GGA+U calculations for the HT phase with $U_{Fe} = U_{Mn} = 4$ eV, typical values used for oxides of Mn and Fe. Figure 2a shows the projected density of states (PDOS) plots calculated for the up- and down-spin 3d states of the Mn and Fe atoms. Each Fe has the $t_{2g}\uparrow$ and $t_{2g}\downarrow$ states fully occupied, while each Mn has the $t_{2g}\uparrow$ states fully occupied and the $e_g\uparrow$ states half-occupied. Because the energy of the occupied Fe t_{2g} states is lower than that of the Mn $e_g\uparrow$ states, charge transfer from the Fe to Mn sites is prevented. To make this charge transfer possible, the Mn $e_g\uparrow$ state should be lowered in energy. The addition of U on a 3d magnetic ion splits its 3d↑ and 3d↓ states such that, with increasing U, the 3d↑ (3d↓) state is further lowered (raised) in energy. Thus, the use of a large U_{Mn} would make charge transfer possible.

To verify the above implication, we first performed GGA+U calculations for various U_{Fe} with $U_{Mn} = 4$ eV (Table 1a) to find that the correct electronic structure of the

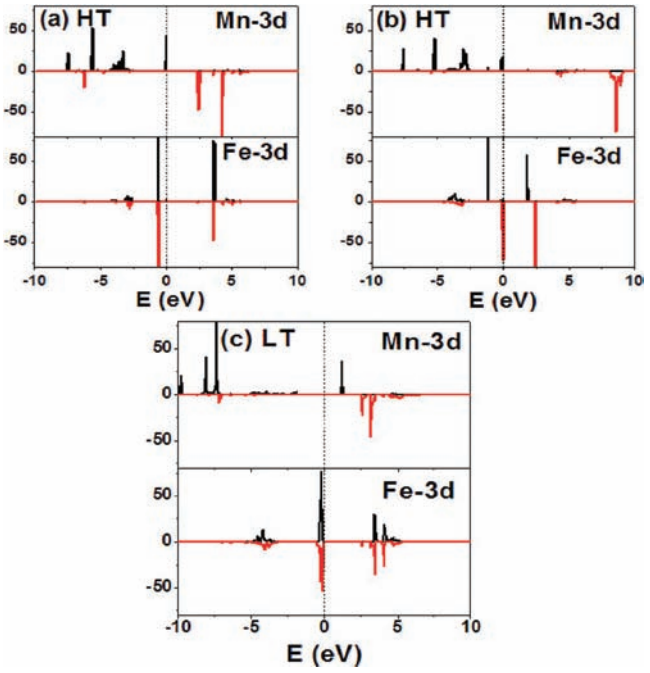

Figure 2. PDOS plots of the Mn and Fe 3d states of $RbMn[Fe(CN)_6]$ obtained from GGA+U calculations for (a) the HT cubic structure with $U_{Mn} = U_{Fe} = 4$ eV, (b) the HT structure with $U_{Mn} = 8$ eV and $U_{Fe} = 1$ eV, and (c) the LT structure with $U_{Mn} = 8$ eV and $U_{Fe} = 1$ eV. The up- and down-spin densities are indicated by positive and negative values, respectively.

Table 1. Spin Moments of the Mn and Fe Sites Obtained for the HT Structure of $RbMn[Fe(CN)_6]$ by GGA+U Calculations

(a) As a Function of U_{Fe} with U_{Mn} Fixed at 4 eV

	U_{Fe} (eV)			
	1	2	4	6
μ_{Mn} (μ_B)	4.01	3.91	3.88	3.89
μ_{Fe} (μ_B)	0.36	0.16	0.04	0.01

(b) As a Function of U_{Mn} with U_{Fe} Fixed at 1 and 2 eV (Results for $U_{Fe} = 2$ eV Are in Parentheses)

	U_{Mn} (eV)		
	4	6	8
μ_{Mn} (μ_B)	4.01 (3.91)	4.30 (4.22)	4.58 (4.53)
μ_{Fe} (μ_B)	0.36 (0.16)	0.64 (0.47)	1.01 (0.89)

HT structure is not obtained even when $U_{Fe} \ll U_{Mn}$. The μ_{Mn} values of Table 1a suggest the need to use $U_{Fe} \ll U_{Mn}$ with small U_{Fe}. Thus, we performed GGA+U calculations for various U_{Mn} with U_{Fe} fixed at 1 and 2 eV. As summarized in Table 1b, μ_{Mn} and μ_{Fe} increase gradually with an increase in the difference $U_{Mn} - U_{Fe}$, reaching values of 4.59 and 1.09 μ_B, respectively, when $U_{Mn} = 8$ eV and $U_{Fe} = 1$ eV. These calculated moments are close to the values expected for the HS Mn^{2+}/LS Fe^{3+} configuration (5 and 1 μ_B, respectively).[4,8,15] The corresponding PDOS plots (Figure 2b) show the expected feature; i.e., each Mn has the $t_{2g}\uparrow$ and $e_g\uparrow$ states fully occupied,

(10) (a) Blöchl, P. E. *Phys. Rev. B* **1994**, *50*, 17953. (b) Kresse, G.; Hafner, J. *Phys. Rev. B* **1994**, *49*, 14251.
(11) Perdew, J. P.; Burke, K.; Ernzerhof, M. *Phys. Rev. Lett.* **1996**, *77*, 3865.
(12) Monkhorst, H. J.; Pack, J. D. *Phys. Rev. B* **1976**, *13*, 5188.
(13) Dudarev, S. L.; Botton, G. A.; Savrasov, S. Y.; Humphreys, C. J.; Sutton, A. P. *Phys. Rev. B* **1998**, *57*, 1505.
(14) Becke, A. D. *J. Chem. Phys.* **1993**, *98*, 5648.

(15) We note that the calculated total moment μ_T per unit cell is close to the sum μ_{sum} of the moments of the four Mn and four Fe atoms. For example, $\mu_T = 22.38\ \mu_B$ and $\mu_{sum} = 22.36\ \mu_B$ for $U_{Mn} = 8$ eV and $U_{Fe} = 1$ eV, while $\mu_T = 17.82\ \mu_B$ and $\mu_{sum} = 17.48\ \mu_B$ for $U_{Mn} = 4$ eV and $U_{Fe} = 1$ eV.

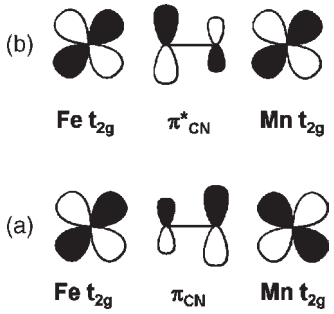

Figure 3. Interaction of the Fe t_{2g} and Mn t_{2g} orbitals with the (a) π_{CN} and (b) π^*_{CN} orbitals of the CN ligand in each Fe−CN−Mn linkage of $RbMn[Fe(CN)_6]$.

Table 2. Spin Moments of the Mn and Fe Sites Obtained for the LT Structure of $RbMn[Fe(CN)_6]$ by GGA+U Calculations for Various Values of U_{Mn} with U_{Fe} Fixed at 1 and 2 eV (Results for U_{Fe} = 2 eV Are in Parentheses)

	U_{Mn} (eV)		
	4	6	8
μ_{Mn} (μ_B)	3.70 (3.71)	3.82 (3.83)	3.93 (3.93)
μ_{Fe} (μ_B)	0.12 (0.12)	0.09 (0.09)	0.07 (0.06)

while each Fe has the $t_{2g}\uparrow$ states fully occupied and the $t_{2g}\downarrow$ states partially unoccupied. Thus, the observed HS Mn^{2+}/LS Fe^{3+} configuration of the HT cubic phase is reproduced only when $U_{Mn} \gg U_{Fe}$ with very small U_{Fe}.

We note that the U_{Mn} and U_{Fe} values appropriate for the HT cubic phase are also valid for the LT tetragonal phase. As summarized in Table 2, μ_{Mn} = 3.93 μ_B and μ_{Mn} = 0.07 μ_B when U_{Mn} = 8 eV and U_{Fe} = 1 eV, which are very close to those expected for the HS Mn^{3+}/LS Fe^{2+} configuration of the LT tetragonal phase (i.e., 4 and 0 μ_B, respectively).[4,8] The PDOS plots calculated for the LT tetragonal phase with U_{Mn} = 8 eV and U_{Fe} = 1 eV show the HS Mn^{3+}/LS Fe^{2+} configuration (Figure 2c). As expected, the HT cubic phase is calculated to be less stable than the LT tetragonal phase (by 2.4 eV per formula unit).

Our finding of $U_{Mn} \gg U_{Fe}$ is quite surprising, and such an observation has not been reported in DFT studies on magnetic oxides of transition-metal elements. In such oxides, the ligands surrounding the transition-metal ions are σ donors. In $RbMn[Fe(CN)_6]$, the CN ligands act as σ donors to both Fe^{n+} and Mn^{n+} (n = 2, 3) ions. In addition, the π_{CN} and π^*_{CN} orbitals of the CN ligands interact with the Fe t_{2g} and Mn t_{2g} orbitals. π_{CN} has a greater weight on the N atom but π^*_{CN} on the C atom (Figure 3). Consequently, the Fe t_{2g}−π^*_{CN} interaction is stronger than the Fe t_{2g}−π_{CN} interaction, whereas the Mn t_{2g}−π^*_{CN} interaction is weaker than the Mn t_{2g}−π_{CN} interaction. Thus, the CN ligands act as π acceptors to the Fe^{n+} ions but as π donors to the Mn^{n+} ions. The π-back-donation effect of the CN ligands on the Fe^{n+} ion, via the Fe t_{2g}−π^*_{CN} interaction, would delocalize the electron density of the Fe^{n+} ion into the CN ligands, hence making the electron distribution around the Fe^{n+} ion less contracted and reducing U_{Fe}. In contrast, the electron distribution around the Mn^{n+} ion would become more contracted because of the π-donation effect of the CN ligands, hence increasing U_{Mn}.

In their study of the experimentally deduced charge-density distribution of $RbMn[Fe(CN)_6]$ using the maximum entropy method,[16] Kato et al. found that, in the charge-transfer transition from the HS Mn^{2+}/LS Fe^{3+} configuration to the HS Mn^{3+}/LS Fe^{2+} configuration, the transferred electron is spread over the complex $[Fe(CN)_6]^{4-}$ because of the Fe t_{2g}−π^*_{CN} interaction, which is consistent with our finding described above.

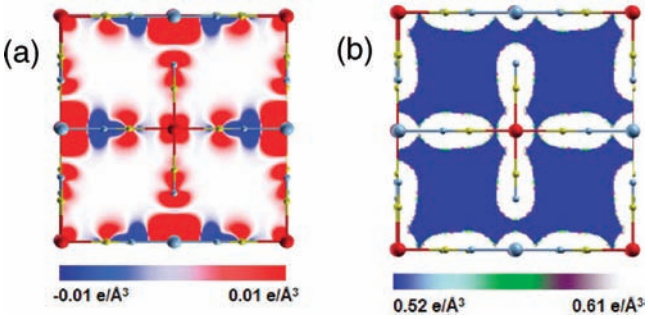

Figure 4. Plots of (a) the spin density and (b) a part of the charge-density distribution obtained for the LT phase of $RbMn[Fe(CN)_6]$ from GGA+U calculations with U_{Mn} = 8 eV and U_{Fe} = 1 eV. The large red and turquoise spheres represent the Fe and Mn atoms, respectively.

The spin-density distribution calculated for the LT phase is presented in Figure 4a. The formally diamagnetic Fe^{2+} ions participate in the spin-density distribution; the Mn^{3+} spins are delocalized into each FeC_6 octahedron plus the N atoms of the two axial CN bonds, while the four equatorial CN bonds exhibit spin polarization.[17] The ferromagnetic coupling between the Mn sites, though separated with a long distance, arises from the spin delocalization through the intervening $Fe(CN)_6$ octahedra, which is caused by Fe t_{2g}−π^*_{CN} interactions. In terms of the charge-density distribution, the occurrence of the electron delocalization between the Fe^{2+} ion and the CN ligands can be seen for a certain range of electron-density values. An example is given in Figure 4b, which shows the electron delocalization between the Fe^{2+} ion and the axial CN ligands.

Compared with the experimental LT and HT structures, their optimized structures by GGA+U calculations (see the Supporting Information) have a shorter (longer) Fe−C (Mn−N) bond and require a smaller U_{Mn} (i.e., 4 eV) for the proper description of the electronic structures. Nevertheless, the requirement for $U_{Fe} \ll U_{Mn}$ with small U_{Fe} remains the same.

In summary, the extent of electron correlation is much greater for the Mn^{n+} ion than for the Fe^{n+} ion (n = 2, 3) in $RbMn[Fe(CN)_6]$ because of the π-back-donation effect of the CN ligands, which delocalizes the electron density of the Fe^{n+} ion into the surrounding CN ligands. This makes the electron distribution around the Fe^{n+} ion less contracted but makes that around the Mn^{n+} ion more contracted. Consequently, U_{Fe} is small and $U_{Mn} \gg U_{Fe}$.

Acknowledgment. The work was supported by the U.S. Department of Energy under Grant DE-FG02-86ER45259 and by the resources of the NERSC and HPC Centers of North Carolina State University.

Supporting Information Available: Optimized and electronic structures of the LT and HT phases. This material is available free of charge via the Internet at http://pubs.acs.org.

(16) Kato, K.; Moritomo, Y.; Tanaka, H.; Tokoro, H.; Ohkoshi, S.; Takata, M. *J. Phys. Soc. Jpn.* **2007**, *76*, 123602.

(17) The negative spin-density contribution from the equatorial N atoms (Figure 4a) will lead to a total measured moment (at saturation) lower than the expected formal value.